The cosmic microwave background and inflation

Martin BUCHER, Laboratoire Astroparticles & Cosmologie,
Université Paris 7 (Denis-Diderot)/CNRS
(for the Planck Collaboration)

3 septembre 2015, Cosmo Cruise, Mediterranean Sea

A Joint Analysis of BICEP2/Keck Array and Planck Data BICEP2/Keck and Planck Collaborations 2015 Submitt

Planck intermediate results. XXX. The angular power spectrum of polarized dust emission at intermediate an
Planck 2015 results. I. Overview of products and results
Planck 2015 results. II. Low Frequency Instrument data processing
Planck 2015 results. III. LFI systematic uncertainties
Planck 2015 results. IV. LFI beams and window functions
Planck 2015 results. V. LFI calibration
Planck 2015 results. VI. LFI maps
Planck 2015 results. VII. High Frequency Instrument data processing: Time-ordered information and beam pro
Planck 2015 results. VIII. High Frequency Instrument data processing: Calibration and maps
Planck 2015 results. IX. Diffuse component separation: CMB maps
Planck 2015 results. X. Diffuse component separation: Foreground maps
Planck 2015 results. XI. CMB power spectra, likelihood, and consistency of cosmological parameters
Planck 2015 results. XII. Simulations Planck Collaboration
Planck 2015 results. XIII. Cosmological parameters
Planck 2015 results. XIV. Dark energy and modified gravity
Planck 2015 results. XV. Gravitational lensing
Planck 2015 results. XVI. Isotropy and statistics of the CMB
Planck 2015 results. XVII. Primordial non-Gaussianity
Planck 2015 results. XVIII. Background geometry and topology of the Universe
Planck 2015 results. XIX. Constraints on primordial magnetic fields
Planck 2015 results. XX. Constraints on inflation
Planck 2015 results. XXI. The integrated Sachs-Wolfe effect
Planck 2015 results. XXII. A map of the thermal Sunyaev-Zeldovich effect
Planck 2015 results. XXIII. Thermal Sunyaev-Zeldovich effect-cosmic infrared background correlation
Planck 2015 results. XXIV. Cosmology from Sunyaev-Zeldovich cluster counts
Planck 2015 results. XXV. Diffuse, low-frequency Galactic foregrounds
Planck 2015 results. XXVI. The Second Planck Catalogue of Compact Sources
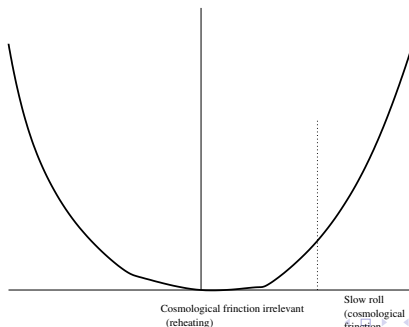Planck 2015 results. XXVII. The Second Planck Catalogue of Sunyaev-Zeldovich Sources
Planck 2015 results. XXVIII. The Planck Catalogue of Galactic Cold Clumps
http://www.cosmos.esa.int/web/planck/publications

Single-Field Inflation

In the beginning there was a scalar field that dominated the universe. Everything came from this scalar field and there was nothing without the scalar field. The quantum fluctuations of this field (that is, those of the vacuum) generated small fluctuations that advanced or retarded the instant of re-heating. These were the seeds of the large-scale structure.

$$\ddot{\phi} + 3H\dot{\phi} = -V_{,\phi}$$

Cosmological frinction irrelevant (reheating)

Slow roll (cosmological frinction

Massless scalar field in de Sitter space

$H_{phys} = (\mathrm{constant})$.

$$ds^2 = -\frac{1}{\eta^2}(-d\eta^2 + d\mathbf{x}^2), \qquad -\infty < \eta < 0.$$

$$S = \int \sqrt{-g}\, g^{\mu\nu}(\partial_\mu\phi)(\partial_\nu\phi) = \int d^4x\; a^2(\eta)\left[\left(\frac{\partial\phi}{\partial\eta}\right)^2 - (\nabla\phi)^2\right]$$

$$\frac{\partial^2\phi}{\partial\eta^2} - \frac{2}{\eta}\frac{\partial\phi}{\partial\eta} + k^2\phi = 0$$

Bessel equation

$$\phi(\eta) = \eta^{3/2}H^{(1)}_{3/2}(-k\eta)$$

$(k\eta) \approx 1$ horizon crossing.

Important points :

▶ Both the inflaton/scalar gravity degrees of freedom and the tensor metric perturbations exhbit the same qualitative behavior as the above idealized example.

▶ Modes fluctuation on subhorizon scales but become frozen in on superhorizon scales and stay frozen in until after the end of inflation.

Perturbations generated during inflation

$$\boxed{\hbar = c = 1, M_{pl}^{-2}} \qquad \delta\phi \approx H \qquad \frac{\delta\rho}{\rho} \approx H \cdot \delta t, \quad \delta t \approx \frac{\delta\phi}{\dot\phi}$$

$$H\dot\phi \approx V_{,\phi}, \quad \dot\phi \approx V_{,\phi}/H, \quad H^2 \approx \frac{1}{M_{pl}^2} V, \frac{\delta\rho}{\rho} \approx \frac{V^{3/2}[\phi(k)]}{M_{pl}^3 V_{,\phi}}$$

Scalar perturbations :
$$\boxed{\mathcal{P}_S^{1/2}(k) \approx O(1) \cdot \frac{V^{3/2}[\phi(k)]}{M_{pl}^3 V_{,\phi}[\phi(k)]}.}$$

Tensor perturbations :
$$\boxed{\mathcal{P}_T^{1/2}(k) \approx O(1) \cdot \frac{H}{M_{pl}} \approx O(1) \cdot \frac{V^{1/2}}{M_{pl}^2}}$$

$\phi(k) \equiv$ value of ϕ at horizon crossing of the mode k

Reconstruction of the inflationary potential : the tensors measure the height of the potential, the scalars the slope.
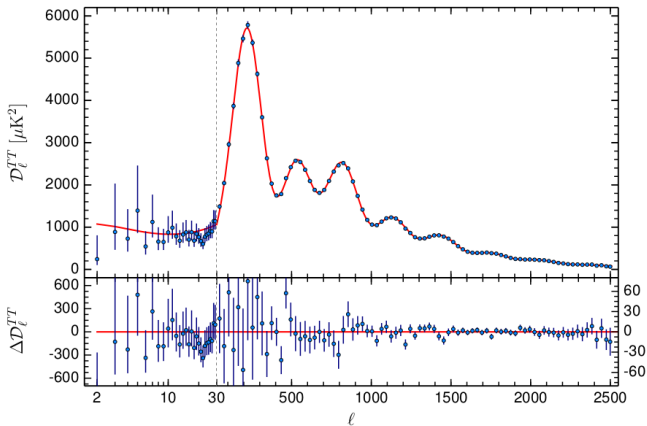
Fig. 1. The *Planck* 2015 temperature power spectrum. At multipoles $\ell \geq 30$ we show the maximum likelihood frequency averaged temperature spectrum computed from the `Plik` cross-half-mission likelihood with foreground and other nuisance parameters determined from the MCMC analysis of the base ΛCDM cosmology. In the multipole range $2 \leq \ell \leq 29$, we plot the power spectrum estimates from the `Commander` component-separation algorithm computed over 94% of the sky. The best-fit base ΛCDM theoretical spectrum fitted to the *Planck* TT+lowP likelihood is plotted in the upper panel. Residuals with respect to this model are shown in the lower panel. The error bars show $\pm 1\,\sigma$ uncertainties.
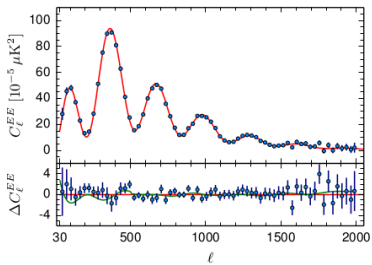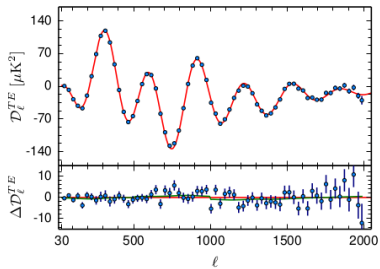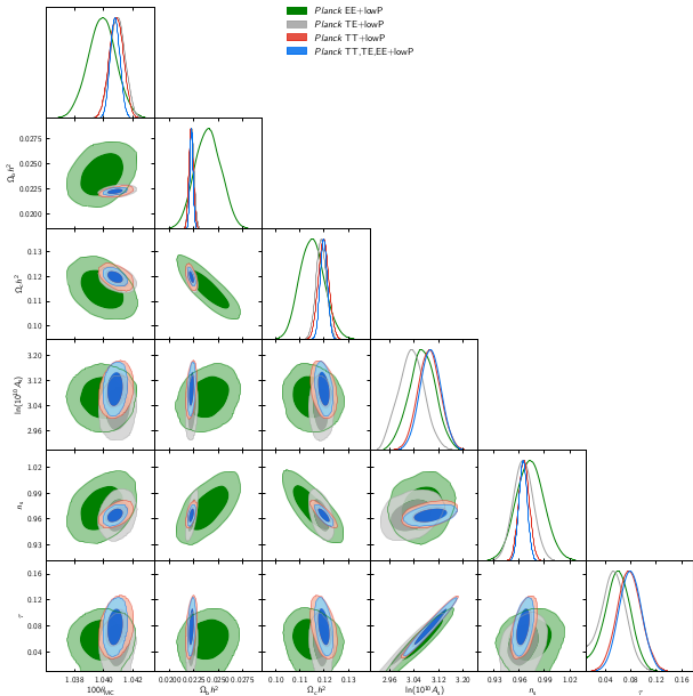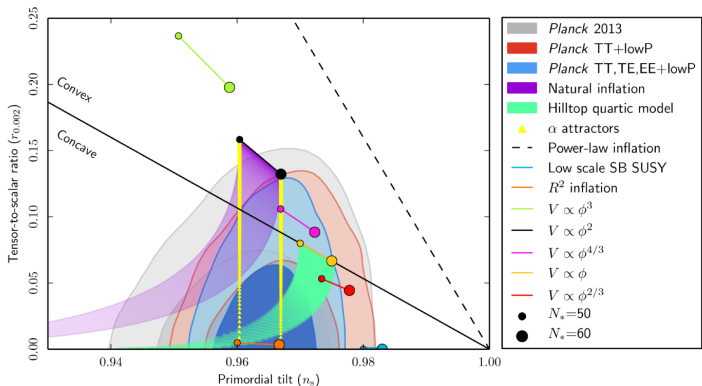
Fig. 12. Marginalized joint 68 % and 95 % CL regions for n_s and $r_{0.002}$ from *Planck* in combination with other data sets, compared to the theoretical predictions of selected inflationary models.

Table 6. Results of the inflationary model comparison. We provide $\Delta\chi^2$ with respect to base ΛCDM and Bayes factors with respect to R^2 inflation.

| Inflationary model	$\Delta\chi^2$		$\ln B_{0X}$	
	$w_{\text{int}} = 0$	$w_{\text{int}} \neq 0$	$w_{\text{int}} = 0$	$w_{\text{int}} \neq 0$
$R + R^2/(6M^2)$	+0.8	+0.3	. . .	+0.7
$n = 2/3$	+6.5	+3.5	−2.4	−2.3
$n = 1$	+6.2	+5.5	−2.1	−1.9
$n = 4/3$	+6.4	+5.5	−2.6	−2.4
$n = 2$	+8.6	+8.1	−4.7	−4.6
$n = 3$	+22.8	+21.7	−11.6	−11.4
$n = 4$	+43.3	+41.7	−23.3	−22.7
Natural	+7.2	+6.5	−2.4	−2.3
Hilltop ($p = 2$)	+4.4	+3.9	−2.6	−2.4
Hilltop ($p = 4$)	+3.7	+3.3	−2.8	−2.6
Double well	+5.5	+5.3	−3.1	−2.3
Brane inflation ($p = 2$)	+3.0	+2.3	−0.7	−0.9
Brane inflation ($p = 4$)	+2.8	+2.3	−0.4	−0.6
Exponential inflation	+0.8	+0.3	−0.7	−0.9
SB SUSY	+0.7	+0.4	−2.2	−1.7
Supersymmetric α-model	+0.7	+0.1	−1.8	−2.0
Superconformal ($m = 1$)	+0.9	+0.8	−2.3	−2.2
Superconformal ($m \neq 1$)	+0.7	+0.5	−2.4	−2.6
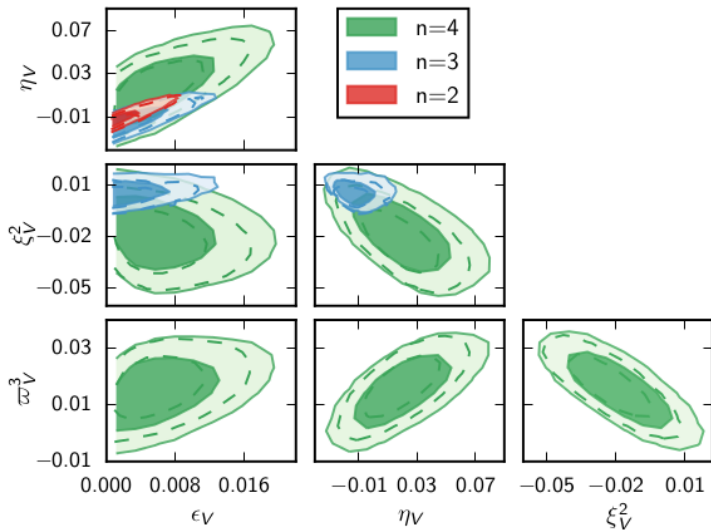
Fig. 13. Posterior distributions for the first four potential slow-roll parameters when the potential is Taylor-expanded to nth order, using *Planck* TT+lowP+BAO (filled contours) or TT,TE,EE+lowP (dashed contours). The primordial spectra are computed *beyond* any slow-roll approximation.
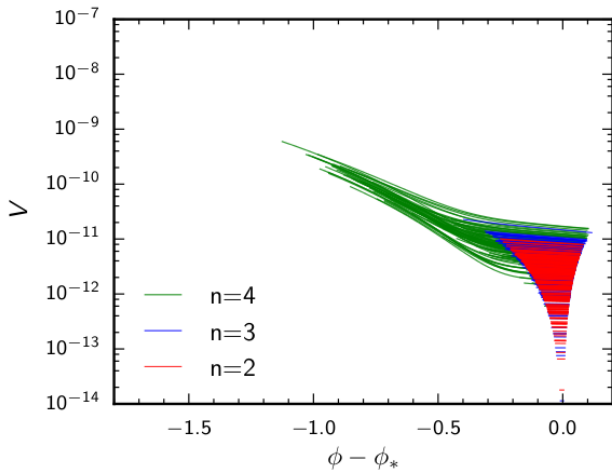
Fig. 15. Observable range of the best-fit inflaton potentials, when $V(\phi)$ is Taylor expanded to the nth order around the pivot value ϕ_*, in natural units (where $\sqrt{8\pi}M_{\mathrm{pl}} = 1$), assuming a flat prior on ϵ_V, η_V, ξ_V^2, and ϖ_V^3, and using *Planck* TT+lowP+BAO. Potentials obtained under the transformation $(\phi - \phi_*) \to (\phi_* - \phi)$ leave the same observable signature and are also allowed. The sparsity of potentials with a small $V_0 = V(\phi_*)$ comes from the flat prior on ϵ_V rather than on $\ln(V_0)$: in fact, V_0 is unbounded from below in

What is the primordial power spectrum ?

▶ For lack of a fundamental theory, expand in powers of $\ln(k)$

$$
\begin{aligned}
\ln\left(\mathcal{P}(\ln k)\right) &= \mathcal{P}_0\left(\ \ln(k/k_{piv})\right)^0 + \mathcal{P}_1\left(\ \ln(k/k_{piv})\right)^1 + \mathcal{P}_2\left(\ \ln(k/k_{piv})\right)^2 + \ldots \\
\mathcal{P}(k) &= A(k/k_{piv})^{(n_s-1)} \\
&\text{or} \\
\mathcal{P}(k) &= A(k/k_{piv})^{(n_s-1)+\alpha\ \ln(k/k_{piv})+\ldots}
\end{aligned}
$$

▶ *Planck* seems to be telling us that the first two terms suffice, and using just the first term can be ruled out at a respectable statistical significance. $n_S \neq 1$ implies exact scale invariance needs to be downgraded to an approximate symmetry. No statistically significant evidence for running of the spectral index.

$$\mathbf{f}^{\mathrm{T}} \mathbf{R}(\lambda, \alpha) \mathbf{f} \equiv \lambda \int \mathrm{d}\kappa \left(\frac{\partial^2 f(\kappa)}{\partial \kappa^2} \right)^2$$

$$+ \alpha \int_{-\infty}^{\kappa_{\min}} \mathrm{d}\kappa \, f^2(\kappa) + \alpha \int_{\kappa_{\max}}^{+\infty} \mathrm{d}\kappa \, f^2(\kappa).$$
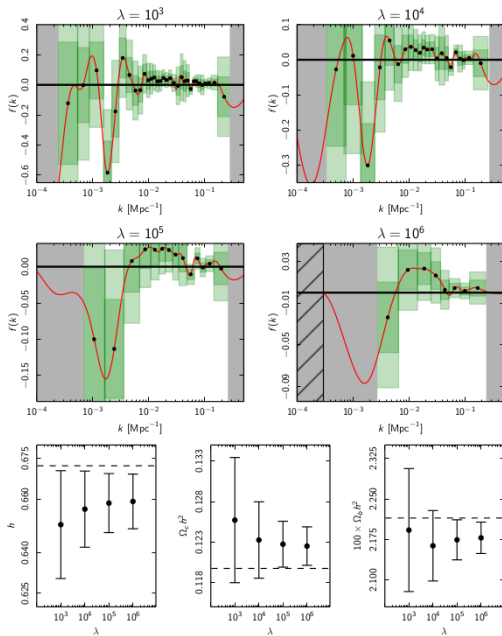
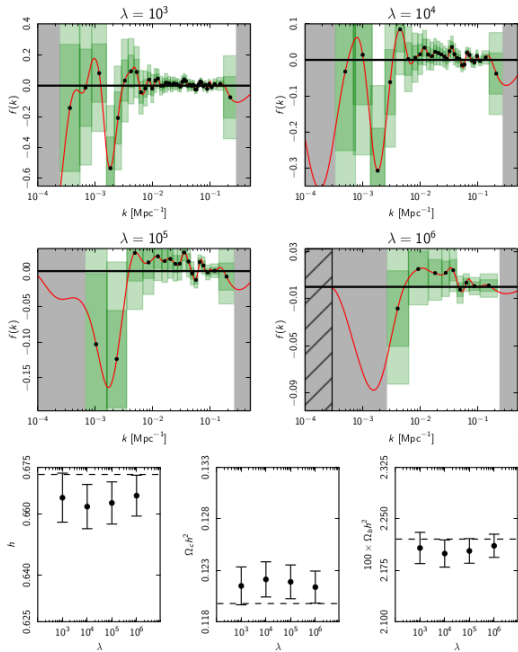**Fig. 21.** *Planck* TT likelihood primordial power spectrum (PPS)

Fig. 22. *Planck* TT,TE,EE+lowTEB likelihood primordial power spectrum reconstruction results. *Top four panels:*
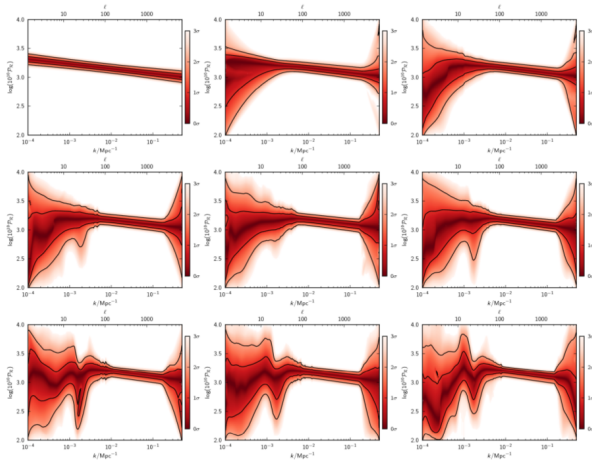
Fig. 24. Bayesian movable knot reconstructions of the primordial power spectrum $\mathcal{P}_{\mathcal{R}}(k)$ using *Planck* TT data. The plots indicate our knowledge of the PPS $P(\mathcal{P}_{\mathcal{R}}(k)|k, N)$ for a given number of knots. The number of internal knots N_{int} increases (left to right and top to bottom) from 0 to 8. For each k-slice, equal colours have equal probabilities. The colour scale is chosen so that darker regions correspond to lower-σ confidence intervals. $1\,\sigma$ and $2\,\sigma$ confidence intervals are also sketched (black curves). The upper horizontal axes give the approximate corresponding multipoles via $\ell \approx k/D_{\text{rec}}$, where D_{rec} is the comoving distance to recombination.
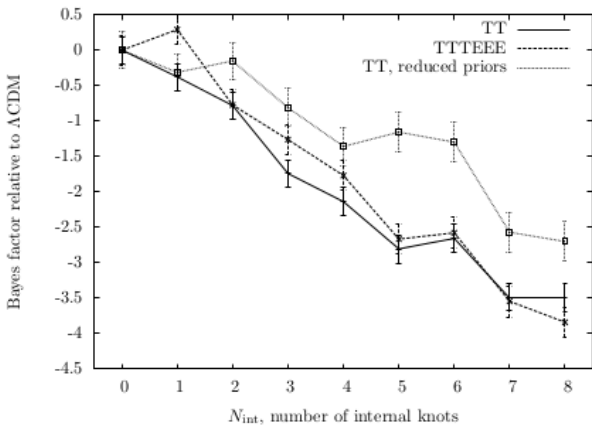
Fig. 25. Bayes factor (relative to the base ΛCDM model) as a function of the number of knots for three separate runs. Solid line: *Planck* TT. Dashed line: *Planck* TT,TE,EE. Dotted line: *Planck* TT, with priors on the $\mathcal{P}$ parameters reduced in width by a factor of 2 ($2.5 < \ln(10^{10}\mathcal{P}) < 3.5$).
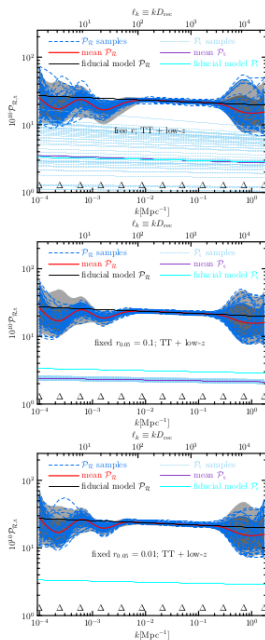
Fig. 27. Reconstructed power spectra applied to the *Planck* 2015 data using 12 knots (with positions marked as Δ at the bottom of each panel) with cubic spline interpolation. Mean spectra as well as sample trajectories are shown for scalars and tensors and

SEARCHING FOR B MODES

E and B Mode Polarization

E mode   B mode

$$\mathbf{Y}_{\ell m, ab}^{(E)} = \sqrt{\frac{2}{(\ell-1)\ell(\ell+1)(\ell+2)}} \left[\nabla_a \nabla_b - \frac{1}{2}\delta_{ab}\nabla^2 \right] Y_{\ell m}(\hat{\Omega})$$

$$\mathbf{Y}_{\ell m, ab}^{(B)} = \sqrt{\frac{2}{(\ell-1)\ell(\ell+1)(\ell+2)}} \frac{1}{2} \left[\epsilon_{ac}\nabla_c\nabla_b + \nabla_a\epsilon_{bc}\nabla_c \right] Y_{\ell m}(\hat{\Omega})$$

Projection of « scalars, »« vectors »and « tensors »onto the celestial sphere

Under projection onto the celestial sphere :

$$(scalar)_3 \rightarrow (scalar)_2,$$

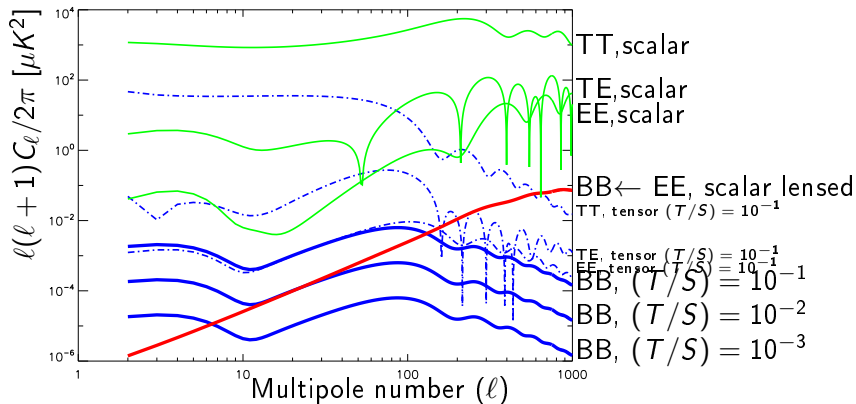$$(vector)_3 \rightarrow (scalar)_2 + (vector)_2,$$

$$(tensor)_3 \rightarrow (scalar)_2 + (vector)_2.$$

There is no $(tensor)_2$ component. The E mode polarization is scalar ; the B mode is vector.
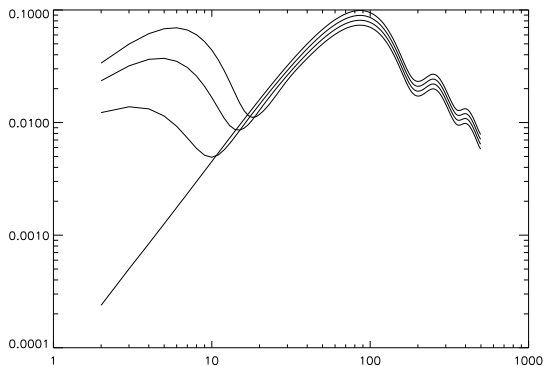
It follows that at linear order the scalar modes cannot generate any B mode polarization.

Note crucial role of linearity assumption.

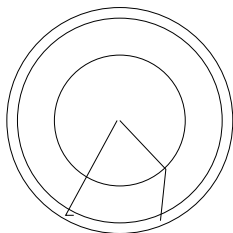# Inflationary Prediction for Scalar & Tensor Anisotropies

The Reionization Bump (I)

$\tau = 0.0, 0.5, 0.10, 0.15$ (bottom → top)

The Reionization Bump (III)

It turns out that

$$P \propto (1 - \tau) d_{lastscatter}^2 \frac{\partial^2 T}{\partial x^2}$$

is small compared to

$$P \propto \tau d_{reion}^2 \frac{\partial^2 T}{\partial x^2}$$

even when τ is small.

Astrophysics

BICEP flexes its muscles

A telescope at the South Pole has made the biggest cosmological discovery so far this century

Mar 22nd 2014 | From the print edition

Timekeeper   Like 204   Tweet 39

Keith Vanderlinde/National Science Foundation

ONE useful feature of a scientific theory is that it makes testable predictions. Such predictions, though, do not have to be testable straight away. Physics is replete with prophecies that could be confirmed or denied only decades later, once the technology to examine them had caught up. The Higgs boson, for example, was 50 years in the confirming.

Stanford Professor Andrei Linde celebrates physics breakthrough

Stanford

369 701

J'aime

Download

À propos de   Partager   Ajouter à

Ajoutée le 17 mars 2014
Assistant Professor Chao-Lin Kuo surprises Professor Andrei Linde
with evidence that supports cosmic inflation theory. The discovery,
made by Kuo and his colleagues at the BICEP2 experiment,
represents the first images of gravitational waves, or ripples in
space-time. These waves have been described as the "first

Plus

The media aftermath

- Around 21 May 2014
  - "We certainly stand by our results."
    —John Kovac, BICEP2 PI, quoted in Scientific American
  - "I wouldn't have held a big press conference about it."
    — Chuck Bennet, WMAP PI, quoted in Scientific American

- A little bit later ($\approx$ 19 June)
  - "Has my confidence gone down ? Yes. . . . Real data from Planck are indicating that our dust models are underestimates. So the prior knowledge on the level of dust at these latitudes, in our field, has gone up ; and so the confidence that there is a gravitational wave component has gone down. Quantifying that is a very hard thing to do. But data trumps models."
    — Clem Pryke, BICEP2 one of the 4 PIs, BBC interview.
  - "[Our] models are not sufficiently constrained by external public data to exclude the possibility of dust emission bright enough to explain the entire excess signal."
    —Revised published version in Physical Review Letters

# Dust is everywhere and must be taken into account
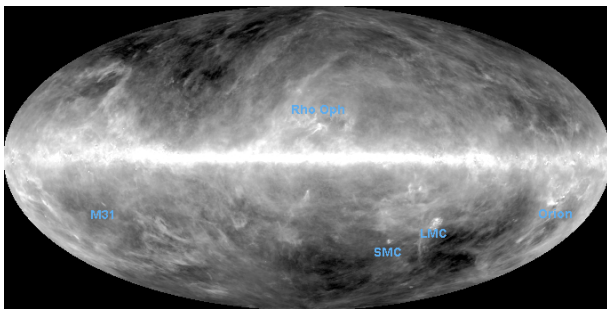
D.J. Schlegel, D.P. Finkbeiner & M. Davis, "Maps of Dust IR Emission for Use in Estimation of Reddening and CMBR Foregrounds" ApJ, 500, 525 (1998)

Combined high-resolution infra-red data at 100μ from IRAS with COBE low-resolution DIRBE maps at 25μ, 100μ, 250μ for better absolute calibration. (Most cited paper of contemporary astronomy).

Competing approach : *HI* column density (measured from 21 cm emission) as a tracer of dust (e.g., Burstein-Heiles map).

Extinction as function of inverse wavelength
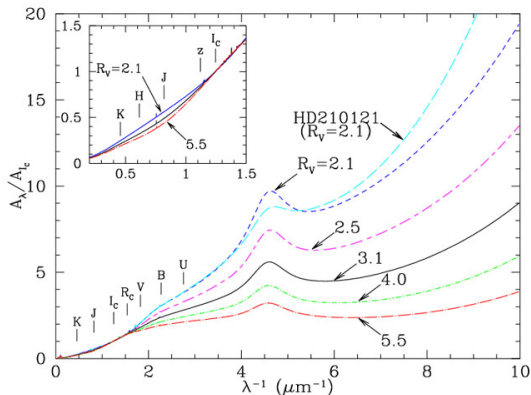
Shape of curve strongly constrains distribution of dust grain sizes
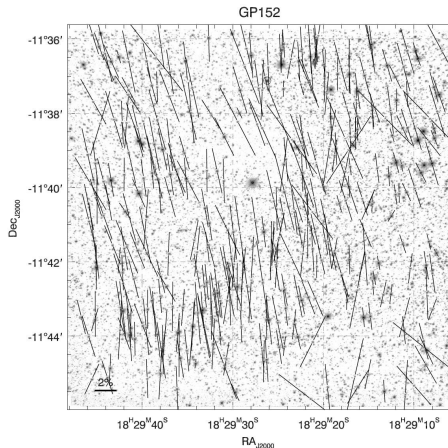
Grain size $\approx 10 - 100$ nm

Mainly carbon, silicon, oxygen with notes of iron, nickel, ...

Two varieties postulated : (1) Carbonaceous (largely graphite ranging to PAHs (polyaromatic hydrocarbons) ;

(2) Silicates

At visible wavelengths starlight polarized at few percent level

(Hiltner and Hall, 1949)

Obvious explanation : dichroism from aligned ellipsoidal dust grain. But what tells them how to align themselves?

Empirical law for thermal dust emission energy spectrum

$$I(\nu) = I_{dust}(\nu/\nu_0)^{\beta} B(\nu; T_{dust}),$$

$$B(\nu; T) = \frac{2h\nu^3}{c^2} \frac{1}{(\exp(h\nu/k_B T) - 1)}.$$

$\chi(\omega)$ is analytic on the lower half-plane. Its poles in the upper half-plane represent the decaying mode excitations of the grain that are coupled to the electromagnetic field. Moreover, on the real axis $\chi(-\omega) = [\chi(+\omega)]^*$. If we assume analyticity in a neighborhood of the origin, we may expand as a power series about the origin so that

$$\chi(\omega) = \omega_0 + i\chi_1\omega + \chi_2\omega^2 + \ldots,$$

and $\chi_0, \chi_1, \chi_2, \ldots$ are all real. It follows that the energy dissipated is characterized by the absorptive cross section

$$\sigma_{abs}(\omega) = 4\pi\omega \mathrm{Im}[\chi(\omega)]/c,$$

and at low frequencies

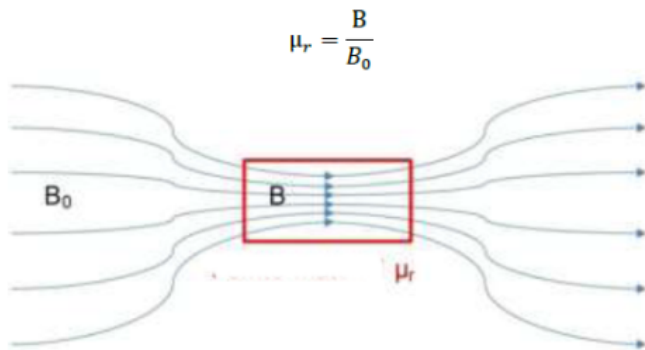$$\sigma_{abs}(\omega) \approx (4\pi\chi^1/c)\omega^2,$$

EM Purcell, "On the Absorption and Emission of Light by Interstellar Grains," Ap. J. 158, 433 (1969)
C Meny et al., "Far-infrared to millimeter astrophysical dust emission I : A model based on physical properties of amorphous solids," Astronomy & Astrophysics, 468 (2007) 171 (astro-ph/0701226)

Naive (non-rotating) alignment explanation

"Compass needle alignment"

$$\mu_r = \frac{B}{B_0}$$
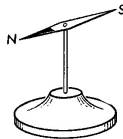
Compass needle alignment (not strong enough given what is known about galactic magnetic fields)

Why do dust grains spin ?

Flippant answer : why not ?

$$\frac{1}{2} I \omega^2 \sim \frac{3}{2} k_B T_{rot}$$
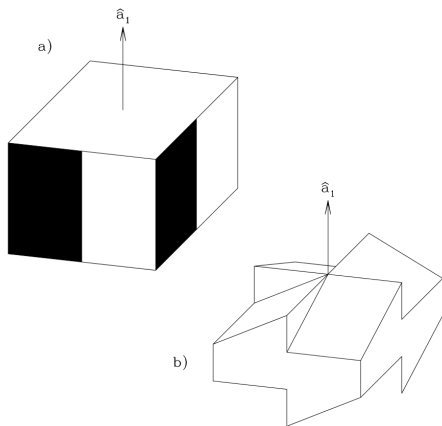
$$\langle \mathbf{\Gamma} \rangle = 0.$$

Fluctuation-dissipation for rotational degree of freedom

$$\dot{\mathbf{L}}(t) = -\alpha \mathbf{L}(t) + \alpha \bar{L} \frac{\mathbf{L}(t)}{|\mathbf{L}(t)|} + \mathbf{\Gamma}_{ran}(t).$$

$$\langle \Gamma_{ran,i}(t) \rangle = 0,$$
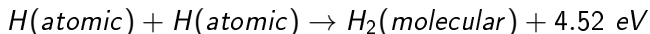$$\langle \Gamma_{ran,i}(t) \, \Gamma_{ran,j}(t') \rangle = \mu_L \, \delta_{ij} \, \delta(t - t')$$

Angular momentum diffusion coefficient has units $[\mu_L] = (\text{Torque})^2/(\text{Time})$.

$$p(\mathbf{L}) = \left(\frac{\beta}{2\pi} \right)^{3/2} \exp \left[-\beta \mathbf{L}^2 \right]$$

From Draine & Weingartner (1997).

$$H(atomic) + H(atomic) \rightarrow H_2(molecular) + 4.52 \ eV$$

- Even though the formation of molecular hydrogen is thermodynamically favored, its formation in vacuum through 2-body interactions proceeds at a negligible rate.
- The grain surface at selected sites is claimed to bring H atoms together and serve as a catalyst.
- A substantial part of the energy released is assumed to be released as kinetic energy of the recoil of the newly formed H_2 molecule.
- For a stochastic distribution of sites on a non-spherical grain these recoil produce a non zero averaged torque—in other words,

$$\langle \mathbf{\Gamma}_{recoil} \rangle \neq 0$$

- Because of the dissipation of angular momentum perpendicular to the axis of largest moment of inertia (assumed to occur faster than the above spin-up), we may simply project the above torque along this principal axis.
- The grain becomes a suprathermal spinning top, described by the orientation of this principal axis and a rotation speed along it.
- So far the mechanism does not favor any particular orientation of the grain, because the torque is biased in the rotating (body) reference frame.
- **A potential drawback (for alignment mechanisms)** : The sites depending on the monolayer structure, which may be expected to change with time as layers are added or eroded away. This is likely to result in **cross-overs** where the projection of $\mathbf{\Gamma}$ onto the largest principal axis changes sign.

Rotation is subtle and full of surprises

Bohr and Pauli observe spinning top

Explorer 1 : First US satellite [(1958) following USSR Sputnik]
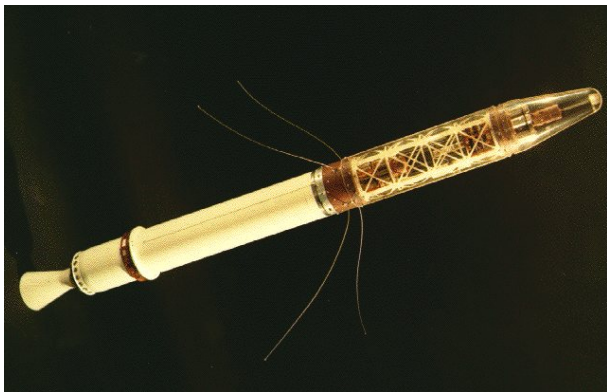
Designed to spin about long axis, but to the surprise of its designers, once in flight, Explorer 1 soon started to spin about an axis at 90°.
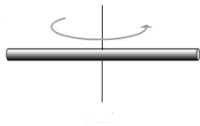Note whisker antennas.

$$I = MR^2/2$$
small moment of inertia,
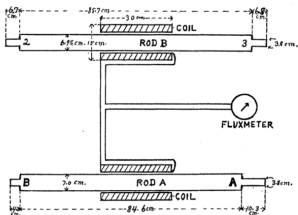high energy

$$I = ML^2/12$$
large moment of inertia,
low energy

$$E = \frac{L^2}{2I}$$

Angular momentum conserved, but excess energy can be dissipated away.

Barnett Effect/Einstein de Haas effect

SJ Barnett, "Magnetization by Rotation," Phys. Rev. 6, 239 (1915)

Iron rod (with high relative magnetic permeability) is made to rotate rapidly and then brought to sudden stop. Assembly carefully shielded from Earth's magnetic field. Rotation aligns the spins inducing a magnetization through spin alignment. When rotation is stopped, spin orientations randomize in order to maximize entropy, and the induced EMF is picked up by the surrounding coil, which is detected by a ballistic galvanometer (which measures integrated current or charge).

Statistical mechanics of spins in a rotating medium

$$\mathbf{J} = \mathbf{L}_{bulk} + \mathbf{S}$$

Energetically, favorable for the spin degrees of freedom to absorb as much of the total angular momentum as possible, because spin alignment entails no energetic cost, but maximizing the entropy favors $\mathbf{S} = 0$.

$$
\begin{aligned}
(\text{Boltzmann factor}) \quad &= \quad \exp\left[\frac{-\beta\mathbf{L}_{bulk}^2}{2I}\right]\exp\left[\mathcal{S}(\mathbf{S})\right] \\
&= \quad \exp\left[+\beta\boldsymbol{\Omega}\cdot\mathbf{S} - a\mathbf{S}^2\right]
\end{aligned}
$$

Ω akin to *chemical potential* for rotation rather than for particle number N. (See, for example, Landau & Lifshitz, Statistical Mechanics).

Irrelevant in macroscopic world unless : (1) Ω is enormous, (2) spins grouped together as in ferromagnetism, so that entropic opposition to alignment is reduced by many orders of magnitude, or (3) the temperature is incredibly low.

Barnett dissipation

$$\dot{\mathbf{L}}(t) \quad = \quad -\alpha\gamma\mathbf{\Omega}(t) + \alpha\gamma^2 \int_0^\infty d\tau \ \exp[-\gamma\tau] \ \mathbf{\Omega}(t-\tau).$$

$$P_{loss}(t) \quad = \quad \mathbf{\Omega}(t) \cdot \dot{\mathbf{L}}(t) = -\gamma I_s \mathbf{\Omega}(t) \cdot \left\{ \mathbf{\Omega}(t) \cdot -\gamma \int_0^\infty dt' \ \exp[-\gamma t'] \mathbf{\Omega}(t-t') \right\},$$

and to obtain the averaged or secular contribution, we decompose $\mathbf{\Omega}(t)$ into harmonic components of amplitude $\mathbf{\Omega}_a$ and frequency ω_a, so that

$$\left\langle \mathbf{\Omega}(t) \cdot \left\{ \mathbf{\Omega}(t) - \gamma \int_0^\infty dt' \ \exp[-\gamma t'] \mathbf{\Omega}(t-t') \right\} \right\rangle = \frac{1}{2} \sum_a \mathbf{\Omega}_a^2 \frac{\omega_a{}^2}{\gamma^2 + \omega_a{}^2}.$$

It follows that

$$\langle P_{loss} \rangle = -\frac{1}{2} I_S \sum_a \mathbf{\Omega}_a^2 \frac{\omega_a{}^2}{\gamma^2 + \omega_a{}^2}.$$
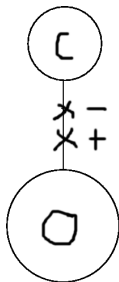
We may obtain an order of magnitude estimate of the alignment rate by assuming that $(\delta I)/I \approx O(1)$ and that except for the stationary component $\omega_a \approx \omega_{max} = L/I_{max}$, so that the excess energy is approximately

$$E_{excess} \approx O(1) \ I_{max} \omega_{max}{}^2 \sin^2 \theta$$

where θ is the disalignment angle, and the rate of dissipation is approximately

$$\bar{P}_{loss} \approx O(1) \ \gamma \ I_S \ \omega_{max}^2 \frac{\omega_{max}{}^2}{\gamma^2 + \omega_{max}{}^2} \sin^2 \theta,$$

Sources of a magnetic moment

- ▶ 1. Barnett effect (described above)
- ▶ 2 Rowland effect. Centers of charge positive and negative charge do not coincide.

  Like CO molecule whose electronic structure is diamagnetic (i.e., completely filled molecular orbitals), but the moments of the electric charge about the COM do not vanish, which absent some symmetry is generically the case.

Davis-Greenstein magnetic dissipation (I)

A component of the angular velocity $\mathbf{\Omega}_\perp$ normal to $\mathbf{B}$ gives rise to an oscillating magnetic field. The magnetic susceptibility at non-zero frequency has a non-zero imaginary part $\chi_{m,i}$:

$$\chi_m(\omega) = \chi_{m,r}(\omega) + i\chi_{m,i}(\omega).$$

Lag in response of the magnetization to driving field gives rise to dissipation, accompanied by a torque that tends to align (or anti-align) the spin with the magnetic field. Effect known as Davis-Greenstein mechanism.

L Davis and J Greenstein, "The Polarization of Starlight by Aligned Dust Grains," Ap. J. 114, 206 (1951)

$$\dot{\mathbf{L}}_\perp = -\frac{1}{\tau_{DG}}\mathbf{L}_\perp, \qquad \dot{\mathbf{L}}_\| = 0$$

Davis-Greenstein magnetic dissipation (II)

We now include random torques.

$$
\begin{aligned}
\dot{\mathbf{L}}_\perp &= -\left(\frac{1}{\tau_{DG}} + \frac{1}{\tau_{coll}}\right)\mathbf{L}_\perp + \tau_{rand}{}^{1/2}\left\{\mathbf{n}(t) - \frac{(\mathbf{n}(t)\cdot\mathbf{L}(t))\mathbf{L}(t)}{\mathbf{L}^2(t)}\right\}, \\
\dot{\mathbf{L}}_\parallel &= -\frac{1}{\tau_{coll}}\mathbf{L}_\parallel + \tau_{rand}{}^{1/2}\frac{(\mathbf{n}(t)\cdot\mathbf{L}(t))\mathbf{L}(t)}{\mathbf{L}^2(t)}
\end{aligned}
$$

where stochastic Gaussian white noise vector field has the unequal time expectation value

$$
\langle n_i(t)\ n_j(t')\ \rangle = \delta_{ij}\ \delta(t-t').
$$

Competition between fluctuation and dissipation, so statistical ensemble resulting after $t \gg \tau_{DG}$, resembles the classical thermal ensemble

$$
p(\mathbf{L}) = \exp\left[-\left(\beta_\parallel L_\parallel{}^2 + \beta_\perp \mathbf{L}_\perp{}^2\right)\right]
$$

Alignment with the magnetic field through precession

ODE for precession about axis $\mathbf{\Omega}$ in competition with alignment about another axis $\hat{\mathbf{n}}$:

$$\dot{\mathbf{L}} = \mathbf{\Omega} \times \mathbf{L} - \gamma(\mathbf{L} - \hat{\mathbf{n}}\bar{L}).$$

Two timescales : Ω^{-1} and γ^{-1}. Primarily interested in fast precession (i.e., $\Omega \gg \gamma$). Linear equation with solution decomposing into stationary part plus transient spiralling in

$$\begin{pmatrix} -\gamma & +\Omega & 0 \\ -\Omega & -\gamma & 0 \\ 0 & 0 & -\gamma \end{pmatrix} \begin{pmatrix} L_{\perp 1} \\ L_{\perp 2} \\ L_{\parallel} \end{pmatrix} = -\gamma \bar{L} \begin{pmatrix} \hat{n}_{\perp 1} \\ \hat{n}_{\perp 2} \\ \hat{n}_{\parallel} \end{pmatrix},$$

Stationary solution :

$$\begin{aligned} L_{\perp 1} &= \frac{\gamma^2}{\gamma^2 + \Omega^2} \bar{L} \, \hat{n}_{\perp 2} - \frac{\gamma\Omega}{\gamma^2 + \Omega^2} \bar{L} \hat{n}_{\perp 1}, \\ L_{\perp 2} &= \frac{\gamma^2}{\gamma^2 + \Omega^2} \bar{L} \, \hat{n}_{\perp 1} + \frac{\gamma\Omega}{\gamma^2 + \Omega^2} \bar{L} \hat{n}_{\perp 2}, \\ L_{\parallel} &= \bar{L} \, \hat{n}_{\parallel}. \end{aligned}$$
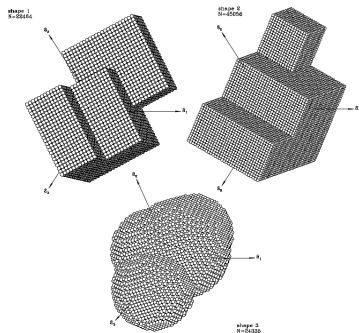
Radiative torques

Fig. 1.—Three representative grain geometries. Shape 1 is the geometry studied in Paper I.

$$\boldsymbol{\Gamma}(t) = \int_0^\infty d\nu \int_{S^2} d\hat{\boldsymbol{n}} \, \boldsymbol{\Gamma}(\nu, \mathcal{R}(t) \circ \hat{\boldsymbol{n}}) I(\nu, \hat{\boldsymbol{n}}).$$

Anisotropic illumination.
(B Draine and J Weingartner, 1997)

Theoretical summary

- Proposals to explain the alignment of interstellar dust grains have a long history. Many of the effects are obvious; others are less so. As the years have passed, new effects not yet taken into account have been pointed out. Perhaps there is still some new physics that has been forgotten.

- Making quantitative theoretical calculations is rendered difficult by our ignorance of the constitution, sizes, and in particular higher-order, parity violating anisotropies of grains. Other grain observables are not sensitive to these crucial details. Grains are likely to be amorphous disordered solids, damaged by cosmic rays. Therefore it is difficult to reproduce faithfully such a grain population in the laboratory.

Worst case scenario vs irrational exuberance

- What is the spectral shape of the I component of the thermal dust emission? It is conventional to use a power law $(\nu/\nu_{ref})^\beta$ to modulate a Planck blackbody spectrum, but if $\beta \neq 2$, there is absolutely no reason to believe that a power law should provide a good fit to the actual emissivity.

- This situation is to be contrasted with galactic synchrotron emission, where the theory is both simple and completely understood. We know that the energy spectrum of the synchrotron emission is smooth because even if the cosmic ray spectrum is jagged, or even δ-function like, it is smoothed by a broad kernel.

- What is the spectral shape of Q and U? It is tempting to speculate that its shape is identical to that of the I spectrum, which is comparatively much simpler to measure. There is no reason to believe that this spectral shape should be the same as for I because alignment is very unlikely to affect all grain populations in exactly the same way.

Dust is likely very complicated.

We still have a lot to learn.

More observations are indispensable.

For a recent overview : Martin Bucher, *Physics of the cosmic microwave background anisotropy*, Published in Int.J.Mod.Phys. D24 (2015) 02, 1530004 (107 pp.) (arXiv :1501.04288) [also to appear as chapter in : *Wei-Tou Ni, Ed., One Hundred Years of General Relativity : From Genesis and Empirical Foundations to Gravitational Waves and Cosmology*, (World Scientifc, Nov 2015)].
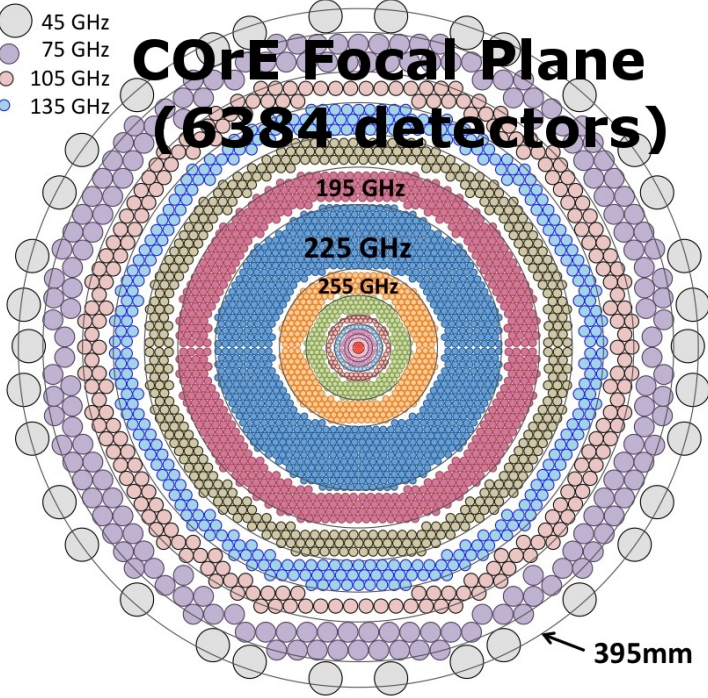
COrE : Cosmic Origins Explorer

A space mission for measuring microwave band polarization on the full sky
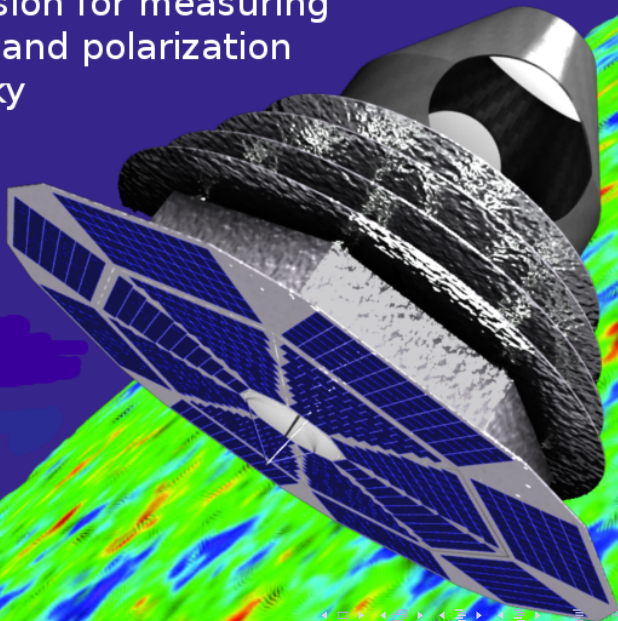
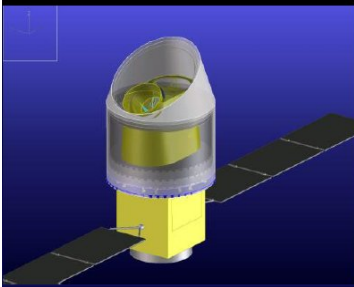COrE Focal Plane
(6384 detectors)

LiteBird Detectors/Resolution

Band	Beam size [degs]	Pixel size[cm]	Edge Taper [dB]	Aperture efficiency	The # of bolometers	uK arcmin for 2 K mirror/baffle
60	1.7	2.0	4.5	0.65	312	6.35
80	1.3	2.0	7.8	0.84	156	6.53
100	1	2.0	<-10	0.94	156	6.06
Sub total					624	
100	1	1.2	-4.5	0.65	434	4.16
150	0.7	1.2	-10	0.91	434	3.02
220	0.47	1.2	<-10	0.99	434	3.02
Sub total					1302	
Total					1926	1.7